PASSIVE FATHOMETRY IN AUSTRALIAN WATERS

Md. Jahangir Alam, Elanor H. Huntington, and Michael R. Frater

School of Engineering and Information Technology,
University College
University of New South Wales
Canberra ACT-2600, Australia

ABSTRACT

Cross-correlation function (CCF) between the ocean ambient noise (OAN) fields received at two hydrophones gives estimate of Green's function (GF) between those two hydrophone positions, which helps in the passive estimation of the bottom profile of the ocean called a passive fathometry. Wind generated ambient noises on the ocean surface mostly contribute to the estimation of passive fathometry. According to the literature this estimation can be improved using broader bandwidth. In the shallow waters near Australia, biological noise is a major component of the broadband OAN field and dominant at low wind speeds because Australian waters are warmer and include a large amount of tropical water which makes them a better place for marine life. In this paper, theoretical analysis of the CCF between OAN fields in the presence of shrimps is presented. The effect of broadband shrimp noise on the passive fathometer is demonstrated using experimental data which shows that in the presence of strong biological activities, only the lower band of the ambient noise is useful in the passive fathometer. Experimental analysis has been performed using both conventional delay and sum (DS) and adaptive minimum variance distortionless response (MVDR) beamforming techniques where the latter technique gives superior estimation.

***Index Terms*—** Passive fathometry, Cross-correlation, Ocean Ambient Noise (OAN), Shrimp, Depth estimation, SNR, Resolution, MVDR, Delay and Sum (DS), Beamforming

1. INTRODUCTION

Bottom profiling of the ocean is one application of geo-acoustic inversion and is performed by cross-correlating the acoustic signals received by the hydrophones[1, 2, 3, 4, 5]. It includes estimating the depths of the ocean's bottom and sub-bottoms which often results in an acoustic image of the seabed.

In a passive technique, the cross-correlation of wind-generated surface noise between two or more hydrophones gives an estimate of the bottom profile of the ocean which is named as "passive fathometry" [1, 6, 7, 8] and based on extracting the Green's Function (GF) from the ambient Noise Cross-correlation Function (NCF) [6]. The GF between two points can be extracted from the derivative of the cross-correlation between the Ocean Ambient Noise (OAN) received at those two points [9, 10, 11]. and the better the estimate of the GF, the better the estimate in the passive fathometer.

Two figures of merit for estimating the GF are the SNR and the resolution of the Cross-Correlation Function (CCF) [12, 10, 13, 14]. One of the requirements of improving the SNR and resolution of the CCF is that a large amount of OAN is needed [10, 13, 15], to collect which there are a number of ways. It has been shown that significant averaging of the NCF is needed for the better estimation of the GF if the noise is recorded at two hydrophones [16, 13, 11, 17, 18, 19, 15], although this requires long recording time. Another way is to use an array of hydrophones in which signals from different pairs of hydrophone are averaged to improve the SNR of the CCF [6, 12, 1]. The number of elements of an array can be increased to increase the SNR of the CCF [6, 20, 13], which makes the array physically large. However, the increase of the number of elements does not increase the resolution of the correlation because the resolution is dependent on the bandwidth of the noise field [9]. However, array processing is limited by the usable bandwidth of the noise field. Until recently, it was thought that the bandwidth cannot be larger than the design frequency of the array [6] due to spatial aliasing, even though the SNR and resolution can be improved by increasing it [12, 14, 13]. Nonetheless, some recent works have shown that this bandwidth can not be increased beyond a certain point due to the adverse effect of shrimp noise, in particular, in Australian waters [21]. This is because OAN generated in shallow Australian waters is dominated by the sound generated by shrimps lying on the seabed and the signals generated by biological activities are considered as overheads in estimations [21]. Passive estimate of ocean depth in Jervis Bay, NSW, Australia in the presence of shrimp noises is analysed in [21] using conventional Delay and Sum (DS) beamforming.

978-0-933957-40-4 ©2013 MTS

This is a DRAFT. As such it may not be cited in other works.
The citable Proceedings of the Conference will be published in
IEEE Xplore shortly after the conclusion of the conference.

In this paper, a comparative experimental analysis of passive depth estimation in Australian waters using conventional DS beamforming and adaptive Minimum Variance Distortionless Response (MVDR) beamforming is presented and it is shown that the latter technique results better estimate than former. This is because, unlike DS beamforming, MVDR beamforming technique concentrates on the vertically propagating signals while rejecting noises coming from other directions [20, 8, 22]. Theoretical analysis presented in [21] is extended in this paper to include off axis wind-generated surface noises and shrimp noises.

Rest of the paper is organised as follows. Section two describes theoretical analysis of passive fathometry in the presence of shrimp noise. Section three explains experimental results and section four concludes the paper.

2. THEORETICAL ANALYSIS

In the passive fathometry, depth of the seabed can be estimated from the delay difference between the direct and the bottom reflected paths of the OAN coming from surface end-fire region and received at two vertically separated hydrophones, if the speed of sound is known [6, 23].

Now, the depth of the sea-bed D is given by

$$D = \frac{\Delta\tau_{dr} \times c + d_s}{2} + d_t \tag{1}$$

where $\Delta\tau_{dr}$ represents the delay difference between direct and bottom reflected paths which can be measured from the NCF [21], d_s is the distance between two consecutive hydrophones and d_t is the depth of the top hydrophone. Speed of sound c can be calculated using equation 2 as

$$\begin{aligned} c = 1449.05 + 45.7(\frac{T_c}{10}) - 5.21(\frac{T_c}{10})^2 + 0.23(\frac{T_c}{10})^3 \\ + (1.333 - 0.126(\frac{T_c}{10}) + 0.009(\frac{T_c}{10})^2)(S_c - 35) \\ + 16.3Z_c + 0.18Z_c^2 \end{aligned} \tag{2}$$

where c, T_c, S_c and Z_c are the speed of sound, water temperature in ^oC, salinity and depth in km respectively.

The passive fathometer described in [21] assumes that only a point noise source from surface end-fire region contribute to the OAN. However, in practice, surface noise sources are uniformly distributed and there are other types of noise sources that contribute to the frequency range of the OAN we are interested in and affect passive fathometer. In this section, we theoretically analyse the CCF of the OAN in the passive fathometer considering off-axis surface noise and biological noise, in particular shrimp noise. Since shrimps usually lie on the seabed in a shallow water area and wind-generated noises are generated in the surface, they will be treated as a sheet of noises on the sea bed and surface respectively. In this analysis, it is considered that wind generated surface noise and shrimp noise contributes linearly to the OAN, which allows to calculate the noise fields and correlations for the shrimp noise and add it to those for the surface noise. Overall noise field and cross-correlation is then given by

$$\phi_\omega = \phi_\omega^{su} + \phi_\omega^{sh} \tag{3}$$

$$C_\omega = C_\omega^{su} + C_\omega^{sh} \tag{4}$$

where ϕ_ω^{su} and ϕ_ω^{sh} are the noise contribution to OAN from surface noise and shrimp noise respectively and C_ω^{su} and C_ω^{sh} are the correlation corresponding to surface noise fields and shrimp noise fields respectively. Mathematical derivations of C_ω^{su} and C_ω^{sh} are demonstrated separately in this section.

2.1. Cross-correlation of surface noise fields

We consider a situation in which uniformly distributed wind-generated surface noises are recorded at two vertically separated hydrophones where hydrophones (S_1 and S_2) positioned at (z_1, r_1) and (z_2, r_2) in a cylindrical coordinate system and, thus, $r_1 = r_2$. The noise fields received at the hydrophones consist of direct signals and reflected signals from the seabed and surface. In the mathematical derivation, only the direct and first bottom-reflected signals are considered to contribute to the noise fields. This is because the first bottom reflection is sufficient to describe the passive fathometer using cross-correlation and subsequent reflections suffer from increased attenuation compared to first bottom reflection, hence little impact on the performance of passive fathometer. The geometry of the noise distribution and its bottom reflection image are shown in Figure 1 [6].

This figure shows that a sheet of noise is generated at z' depth below the surface and a bottom image at $2D - z'$ depth from the surface, where D is the depth of the seabed. Here, the seabed is considered as a rigid body which means that its acoustic impedance is higher than that of the water and, thus, there is no phase change in the reflected signals [24]. The noises coming from all over the surface contribute to the noise fields received at the two hydrophones (S_1 and S_2)) and these two noise fields are a function of the GF retrieved from them. The GFs can be obtained using the method of images [6, 23].

It is considered that random surface noise sources are placed at (r', z') points of the noise plane in the cylindrical coordinate which is denoted as $S_\omega^{su}(r')$ in the frequency domain, where the horizontal displacement is $r' = (x', y')$. The source function ($S_\omega^{su}(r')$) is not dependent on the depth of the noise plane (z'), because z' is constant for all the noise sources.

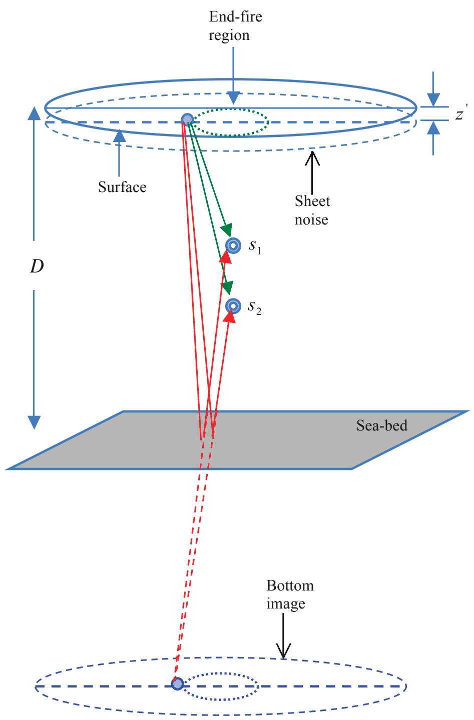

Fig. 1. Geometry of surface noise distribution and image formulation [6]

The noise field ($\phi_\omega^{su}(r,z)$) at point (r,z) due to all the noise sources from the surface noise plane is [6, 25]

$$\phi_\omega^{su}(r,z) = \int S_\omega^{su}(r')G_\omega^{su}(r,r',z,z')dr'$$

where $G_\omega^{su}(r,r',z,z')$ is the GF for surface noise plane.

The noise fields received at hydrophones S_1 and S_2 for the sheet noise sources at the depth of z' are expressed as

$$\phi_\omega^{su}(r_1,z_1) = \int S_\omega^{su}(r')G_\omega^{su}(r_1,r',z_1,z')dr' \quad (5)$$

$$\phi_\omega^{su}(r_2,z_2) = \int S_\omega^{su}(r'')G_\omega^{su}(r_2,r'',z_2,z')dr'' \quad (6)$$

where $G_\omega^{su}(r_1,r',z_1,z')$ and $G_\omega^{su}(r_2,r'',z_2,z')$ are the GFs at hydrophones S_1 and S_2 for the sheet surface noise source which can be represented in integral representation as

$$G_\omega^{su}(r_1,r',z_1,z') = \frac{1}{2\pi}\int G_\omega^{su}(k,z_1,z')e^{[iK(r_1-r')]}dK \quad (7)$$

$$G_\omega^{su}(r_2,r'',z_2,z') = \frac{1}{2\pi}\int G_\omega^{su}(k',z_2,z')e^{[iK(r_2-r'')]}dK' \quad (8)$$

where $G_\omega^{su}(k,z_1,z')$ and $G_\omega^{su}(k',z_2,z')$ are the GFs at hydrophones S_1 and S_2 respectively in the wavenumber domain.

Therefore, the noise fields of equation 5 and 6 can be expressed as

$$\phi_\omega^{su}(r_1,z_1) = \tfrac{1}{2\pi}\int S_\omega^{su}(r')\int G_\omega^{su}(k,z_1,z')e^{[iK(r_1-r')]}dKdr' \quad (9)$$

$$\phi_\omega^{su}(r_2,z_2) = \tfrac{1}{2\pi}\int S_\omega^{su}(r'')\int G_\omega^{su}(k',z_2,z')e^{[iK(r_2-r'')]}dK'dr'' \quad (10)$$

The cross-spectral density is simply the ensemble average of the multiplication of two frequency domain noise fields after conjugating one. Therefore, the cross-spectral density ($C_\omega^{su}(r_1,r_2,z_1,z_2)$) of the noise fields received at S_1 and S_2 is expressed as

$$\begin{aligned} C_\omega^{su}(r_1,r_2,z_1,z_2) &=< \phi_\omega^{su}(r_1,z_1)\times\phi_\omega^{su}(r_2,z_2)^* > \\ &= \frac{1}{(2\pi)^2}\int\int < S_\omega^{su}(r')S_\omega^{su}(r'')^{conj} > dr'dr''\left[\int G_\omega^{su}(k,z_1,z')e^{[iK(r_1-r')]}dK\right] \\ &\times\left[\int S_\omega^{su}(r'')\int G_\omega^{su}(k',z_2,z')e^{[iK(r_2-r'')]}dK'\right]^* \end{aligned} \quad (11)$$

where $*$ in the superscript indicates complex conjugate operation. In equation 11, $< S_\omega^{su}(r')S_\omega^{su}(r'')^{conj} >$ is the correlation function of the surface noise sources denoted as $N^{su}(s)$ which is spatially dependent on only the separation $(s = r' - r'')$. Now, by expressing the noise field points through the difference between the displacement vectors, that is, $R_r = r_1 - r_2$, the cross-spectral density can be denoted as $C_\omega^{su}(R_r,z_1,z_2)$ and expressed as [25]

$$\begin{aligned} C_\omega^{su}(R_r,z_1,z_2) =& \frac{8\pi^2q^2}{k^2(z')}\int_0^\infty G_\omega^{su}(k_r,z_1,z')G_\omega^{su}(k_r,z_2,z')^* \\ & J_0(k_r|R_r|)k_rdk_r \end{aligned} \quad (12)$$

where q^2 is considered the strength of the source function and correlation function can be expressed in the form of a delta function as [26]

$$N^{su}(s) = \frac{4\pi\delta(s)}{k^2(z')}. \quad (13)$$

The Bessel function $J_0(k_r,R_r) = 1$ for the vertically separated hydrophones that disappears from equation 12 due to the use of a vertical array of hydrophones in the passive fathometer.

Considering the source at $z = z'$ and a bottom image of the source at $z = 2D - z'$, the GFs at hydrophones S_1 and S_2 are expressed as [23]

$$G_\omega^{su}(k_r,z_1,z') = \frac{e^{ik_z(z_1-z')}}{4\pi ik_z} + \frac{e^{ik_z[(D-z_1)+(D-z')]}}{4\pi ik_z} \quad (14)$$

$$G^{su}_{\omega}(k_r, z_2, z') = \frac{e^{ik_z(z_2-z')}}{4\pi i k_z} + \frac{e^{ik_z[(D-z_2)+(D-z')]}}{4\pi i k_z}\ . \quad (15)$$

Substituting the expressions of the GFs from equations (14) and (15) in equation (12), the cross-spectral density can be expressed as

$$C^{su}_{\omega}(z_1, z_2) = \frac{8\pi^2 q^2}{k^2(z')(4\pi)^2}\int_0^{\infty}\left[\frac{e^{ik_z(z_1-z_2)}}{k_z^2} + \frac{e^{ik_z[(z_1+z_2-2D)]}}{k_z^2} + \frac{e^{ik_z[(2D-z_1-z_2)]}}{k_z^2} + \frac{e^{ik_z(z_2-z_1)}}{k_z^2}\right]k_r dk_r \quad (16)$$

The vertical wavenumber, k_z, can be defined as $k_z = \sqrt{k^2 - k_r^2}$. After changing the dependent variable from k_r to k_z, the cross-spectral density in equation 16 can be expressed as

$$\begin{aligned} C^{su}_{\omega}(z_1, z_2) &= \frac{-q^2}{4k^2(z')}\int_0^{k}\left[\frac{e^{ik_z(z_1-z_2)}}{k_z^2} + \frac{e^{ik_z[(z_1+z_2-2D)]}}{k_z^2} + \frac{e^{ik_z[(2D-z_1-z_2)]}}{k_z^2} + \frac{e^{ik_z(z_2-z_1)}}{k_z^2}\right]k_z dk_z \\ &= \frac{-q^2}{4k^2(z')}\int_0^{k}\left[\frac{e^{ik_z(z_1-z_2)}}{k_z} + \frac{e^{ik_z[(z_1+z_2-2D)]}}{k_z} + \frac{e^{ik_z[(2D-z_1-z_2)]}}{k_z} + \frac{e^{ik_z(z_2-z_1)}}{k_z}\right]dk_z \end{aligned} \quad (17)$$

2.2. Cross-correlation of shrimp noise fields

In this analysis, direct and first surface reflected paths from shrimp noises are considered to be received by the hydrophone array, as although other paths are available, they are weak in comparison. A shrimp noise sheet and its surface image are considered at $z = D$ and $z = -D$ respectively as shown in Figure 2.

The noise signals generated by shrimps and received at hydrophones S_1 and S_2 can be expressed as

$$\phi^{sh}_{\omega}(r_1, z_1) = \frac{1}{2\pi}\int S^{sh}_{\omega}(r')\int G^{sh}_{\omega}(k, z_1, D)e^{[iK(r_1-r')]}dK dr' \quad (18)$$

$$\phi^{sh}_{\omega}(r_2, z_2) = \frac{1}{2\pi}\int S^{sh}_{\omega}(r'')\int G^{sh}_{\omega}(k', z_2, D)e^{[iK(r_2-r'')]}dK' dr'' \quad (19)$$

The superscript sh represents quantities arising from noise generated by shrimps.

From equations 11 to 12, the cross-spectral density can be expressed as

$$C^{sh}_{\omega}(R_r, z_1, z_2) = \int q^2 N^{sh}(s)e^{-iKs}ds\int G^{sh}_{\omega}(k_r, z_1, D)G^{s}(k_r, z_2, D)^{*} J_0(k_r|R_r|)k_r dk_r \quad (20)$$

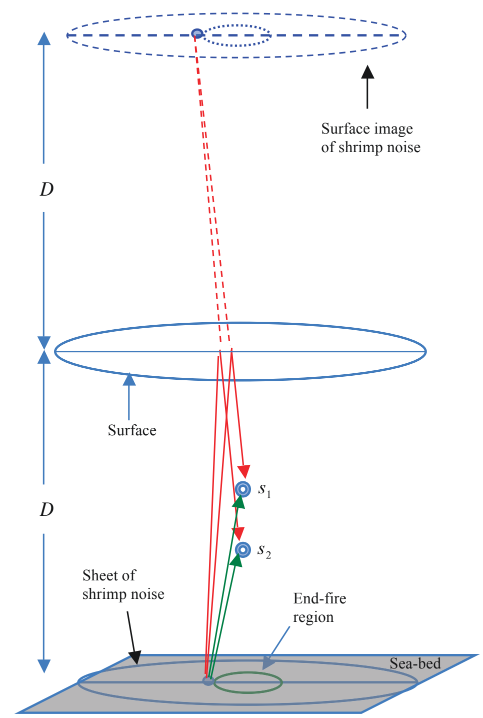

Fig. 2. Geometry of shrimp noise distribution and image formulation

where $N_s(s)$ is the source correlation function of the shrimp noise field. Considering a sheet of shrimps at $z = D$ and its surface image at $z = -D$, the GFs at hydrophones S_1 and S_2 are expressed as

$$G^{sh}_{\omega}(k_r, z_1, D) = \frac{e^{ik_z(D-z_1)}}{4\pi i k_z} - \frac{e^{ik_z(D+z_1)}}{4\pi i k_z} \quad (21)$$

$$G^{sh}_{\omega}(k_r, z_2, D) = \frac{e^{ik_z(D-z_2)}}{4\pi i k_z} - \frac{e^{ik_z(D+z_2)}}{4\pi i k_z}\ . \quad (22)$$

A negative sign in the second term of the GF is observed because of the phase change in the surface-reflected signal [25].

Substituting the expressions for the GFs from equations 21 and 22 in equation 20 and changing the dependent variable from k_r to k_z, the cross spectral density due to shrimp noise fields can be rewritten as

$$C_\omega^{sh}(R_r, z_1, z_2) = \int q^2 N^{sh}(s) e^{-iKs} ds \int_0^k \frac{-1}{2\times(4\pi k_z)^2} \left[e^{ik_z(z_2-z_1)} - e^{-ik_z(z_1+z_2)} - e^{ik_z(z_1+z_2)} + e^{ik_z(z_1-z_2)} \right] k_z dk_z \tag{23}$$

Considering the signal generated by shrimp as a series of impulses, the correlation function $N^{sh}(s)$ is expressed as

$$\begin{aligned} N^{sh}(s) =& N_p\delta(s) + \sum_{i=2}^{N_p}\sum_{j=i}^{N_p} \delta(s + d_j^{click} - d_{i-1}^{click}) \\ &+ \sum_{i=2}^{N_p}\sum_{j=i}^{N_p} \delta(s + d_{N_p-j+1}^{click} - d_{N_p-i+2}^{click}) \end{aligned} \tag{24}$$

where the signal produced by a shrimp consists of N_p number of clicks and is given by

$$\sum_{i=1}^{N_p} \delta(d_i^{click}) \tag{25}$$

where d_i^{click} is the position of the i_{th} click in the shrimp signal.

Figure 3 shows the conceptual graphical sketch of $N^{sh}(s)$ along with the received signals produced by a shrimp. Horizontal axis of the sketches are expressed in distance.

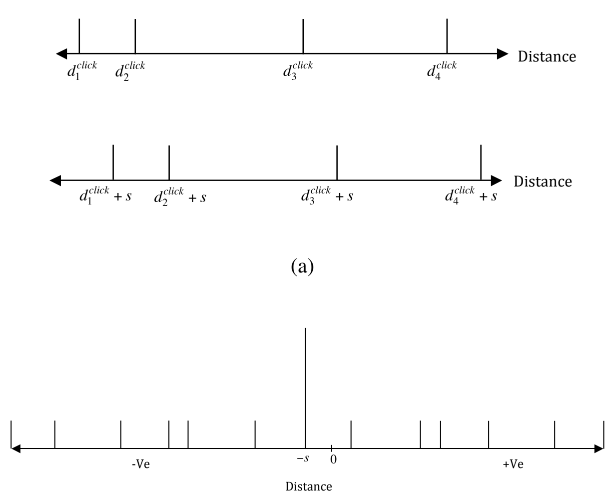

(a)

(b)

Fig. 3. (a) represents signal produced by a shrimp received at S_1 (top) and S_2 (bottom); and (b) represents cross-correlation between them

Figure 3(a) shows signals coming from a single shrimp received at S_1 and S_2 where signal received by S_2 traverse s distance more than S_1 and Figure 3(b) represents the correlation between them. In Figure 3(b), the longest peak generated at $-s$ position represents the first term of equation 24. The other peaks in positive and negative directions represent the second and third terms of equation 24 respectively.

2.3. Cross-correlation of combined noise fields

Now, considering that the combined noise field consists of wind-generated surface noise and shrimp-generated bottom noise, and using equations 12 and 20, the cross-spectral density is given by

$$\begin{aligned} C_\omega(R_r, z_1, z_2) =& \frac{q^2}{2k^2(z')} \int_0^\infty G_\omega^{su}(k_r, z_1, z') G_\omega^{su}(k_r, z_2, z')^* k_r dk_r \\ &+ \int q^2 N^{sh}(s) e^{-iKs} ds \int_0^\infty G_\omega^{sh}(k_r, z_1, D) G_\omega^{sh}(k_r, z_2, D)^* k_r dk_r \\ &+ \int q^2 N^{su-sh}(s) e^{-iKs} ds \int_0^\infty G_\omega^{su}(k_r, z_1, z') G_\omega^{sh}(k_r, z_2, D)^* k_r dk_r \\ &+ \int q^2 N^{su-sh}(s) e^{-iKs} ds \int_0^\infty G_\omega^{sh}(k_r, z_1, D) G_\omega^{su}(k_r, z_2, z')^* k_r dk_r \end{aligned} \tag{26}$$

where $N^{su-sh}()$ represents the source correlation between the wind-generated surface noise field and shrimp-generated bottom noise field. Since these fields can be approximated as random noise and an impulse-like signal respectively, $N^{su-sh}()$ is actually a random signal. The third and fourth terms in equation 26 are the main contributors to the noise part of the overall cross-correlation which implies that the SNR will be worse than previously thought. The first and second terms are derived from equations 23 and 17 and represent the correlation peaks generated in the overall cross-correlation which implies a spurious peak that does not contribute usefully to bottom profiling.

3. EXPERIMENTAL ANALYSIS

Experiment has been conducted at shallow water near Jervis bay, NSW, Australia where seabed is rocky and depth measured by an active sonar (Lowrance GlobalMap 3500c) is 15.2m. A 4-hydrophone array is deployed underwater with the bottom hydrophone at a depth of about 6.5 m from the surface and the spacing between consecutive hydrophones 50 cm. Bruel and Kjaer 8104 hydrophones are attached to a 5.5m long nylon rope of 8mm diameter using duct tape to form an array which is hung from a float on the surface using 1 m long shock cord. A PVC plate of diameter 0.5m is also hung horizontally from the bottom part of the array to prevent the movement of the plate on the effect of surface fluctuation. Since the strength of OAN is low, a RESON VP2000 voltage pre-amplifier with a 50 dB gain is used to amplify the ocean noise before recording. Each 50 s of data slot is recorded at a sampling rate of 192 ksps and the data acquisition device UA101 captures the OAN. The UA101 has 10 input channels, four of which are used to record four channels of data simultaneously. The experimental setup is shown in Figure 4.

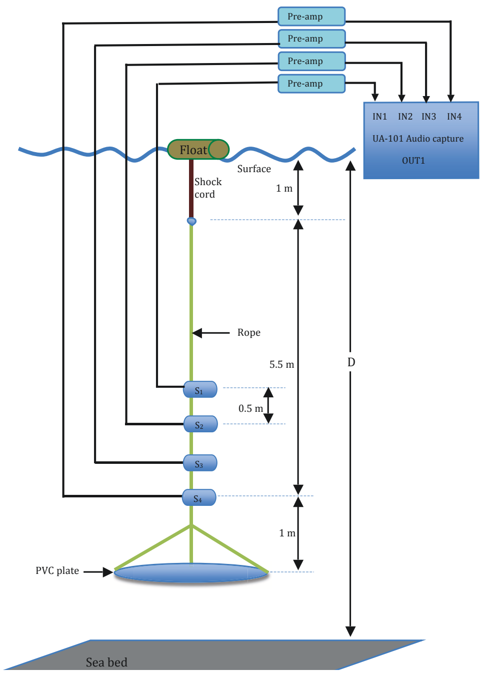

Fig. 4. Experimental setup

The array setup used in the experiment is shown in Figure 5.

A temperature sensor is also deployed at the same depth of the array to measure water temperature at that place which is used to calculate the speed of sound. The speed of sound is calculated using equation 2 where the temperature at the location of the experiment is 20^oC measured by temperature sensor, the salinity of the water is 35.30 PSU [27] and the depth of the measurement is 5m. Using these parameters, speed of sound is calculated as 1521.9 m/s.

Since depth at the experimental location is 15.2 m and the hydrophones S_1 and S_2 are about 5 and 5.5 m below the surface respectively, the delay difference between the direct path at one hydrophone and reflected path at the other is 13.1 ms.

The CCF of the equalised OAN fields of bandwidths (1kHz-20kHz) are processed using both DS and MVDR beamforming techniques and shown in Figure 6.

Results show that large bandwidth (1-20kHz) noise fields does not give estimation of the depth, in particular at Australian shallow water due to the presence of strong sounds

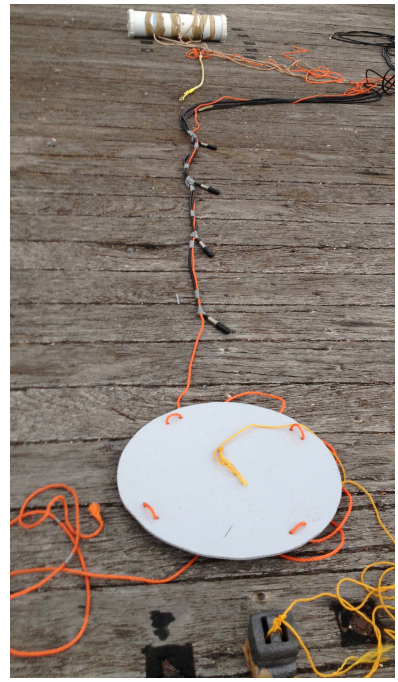

Fig. 5. Array used in the experiment; the equipment is laid out in same order as fig 4 with S_1 at the top of the photograph

produced by shrimps which resembles with the experimental results shown in [21].

Because of the strong biological noise at higher frequencies, only the lower band of the OAN may be used to test the passive fathometer. M. Siderius used the passive fathometer with a frequency band of 200 to 1500 Hz and DS beamforming with an array of 32 elements to estimate the bottom profile of the ocean [6]. For comparison purposes, we use the same lower frequency band in this analysis. A bandpass filter (200-1500 Hz) is applied very carefully on the received noise field because, if applied directly to the noise field of the high bandwidth (96 kHz), it might be numerically unstable. Therefore, the received noise fields are low-pass filtered and then downsampled at the ratio of 10:1 to achieve an effective bandwidth of the noise field of 9.6 kHz and a sampling rate of 19.2 ksps which helps to take the noise field of the frequency band from 200 to 1500 Hz.

After applying DS beamforming using the four hydrophones in the array, the resultant cross-correlation of the equalised noise fields (200-1500 Hz) is shown in Figure 7.

In this beamforming, hydrophone S_1 is used as reference which results a path difference of 20m between direct and reflected paths at S_1. Therefore, a correlation peak is expected at about 13.40 ms away from the correlation centre after beamforming. Although figure 7 shows a correlation peak at about 13.5 ms, a strong low-frequency signal can still be observed in the correlation because delay and sum

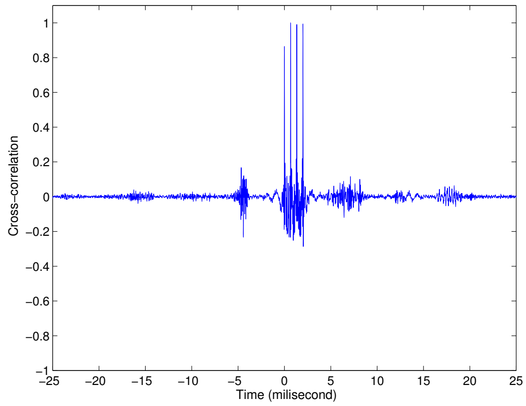

(a)

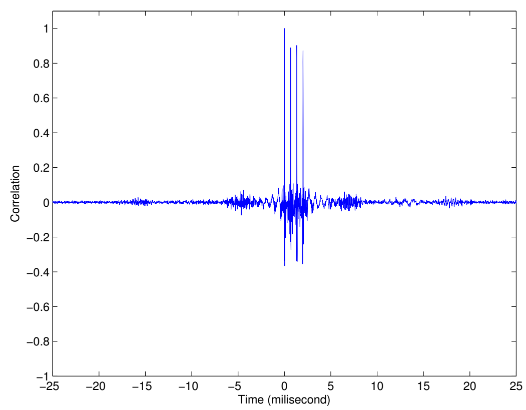

(b)

Fig. 6. (a) and (b) represent cross-correlations of equalised noise fields of 1-20kHz using DS and MVDR beamforming respectively

beamforming cannot remove strong horizontally propagating low-frequency signals from the noise field. However, MVDR beamforming can overcome this problem and a time domain cross-correlation after adaptive processing is shown in Figure 8.

Figure 8 shows a correlation peak at about 13.5 ms with a better SNR than that shown in Figure 7. In Figure 8, four strong correlation peaks are also observed near correlation centre where two consecutive peaks are 0.67ms apart. These peaks are generated due to the correlation of direct path signals coming from end-fire region on the surface while performing correlation between upward and downward beams in MVDR beamforming. This is because, a part of strong direct path signal is present in the upward beam as leakage along with bottom reflected signals. Ringing produced by these four strong peaks interfere with the peak representing depth as shown in Figure 8. This interference can be recov-

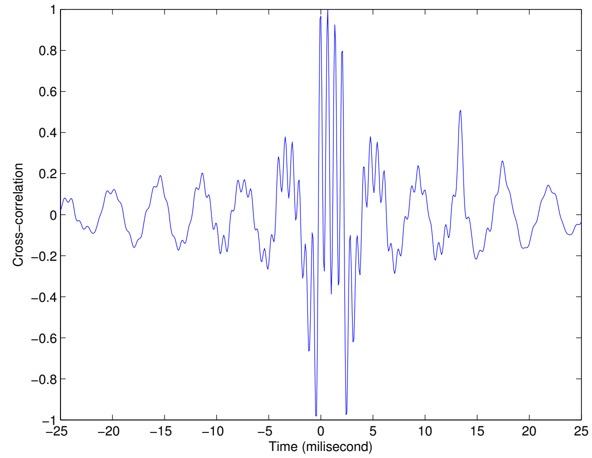

Fig. 7. Cross-correlation of equalised noise fields (200-1500 Hz) after DS beamforming using 4-hydrophone array

ered either with an increase of ocean depth or by placing the array at a shallower depth because the correlation peak representing ocean depth moves away from correlation centre in both of those cases.

The depth of the ocean can be estimated from equation 1 as

$$\frac{20.54 + 0}{2} + 5 = 15.27 \text{ m}$$

where d_t=5 m, Δd_{dr}=20.54 m and d_s=0 for reference hydrophone S_1.

Since five different sets of data have been recorded, estimations from all of them are shown in table 1.

Table 1. Depth estimation from different sets of data

Data set	Position of correlation peak representing depth (ms)	Estimated depth (m)	Errors (m)
1	13.5	15.27	0.07
2	13.58	15.33	0.13
3	13.58	15.33	0.13
4	13.42	15.20	0
5	13.42	15.20	0

Standard deviation of the estimations from different sets

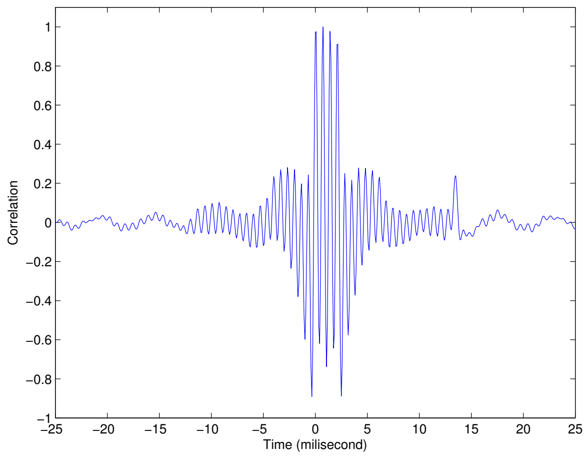

Fig. 8. Cross-correlation of equalised noise fields (200-1500 Hz) after MVDR beamforming using 4-hydrophone array

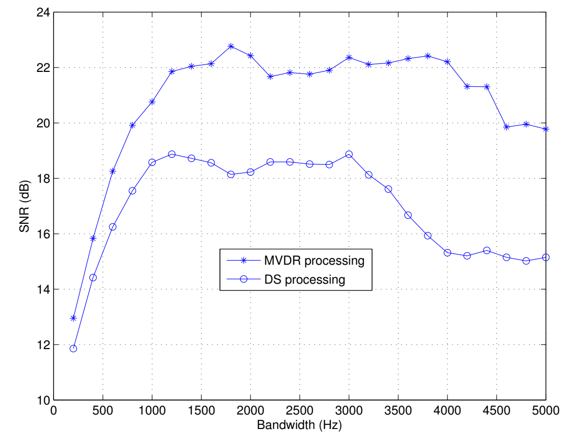

(a) SNR vs bandwidth

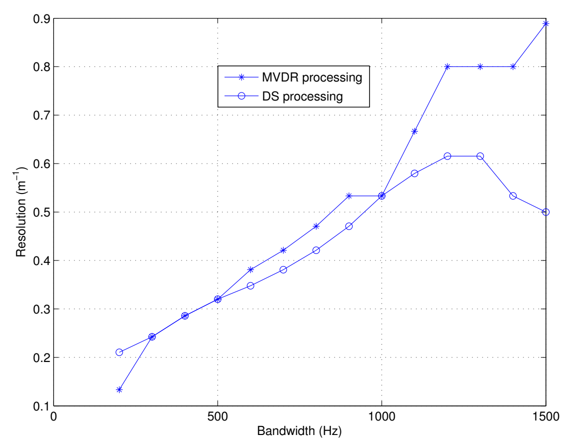

(b) resolution vs bandwidth

Fig. 9. Experimental SNR and resolution of correlation function with respect to bandwidth

of data is 0.065m and mean measurement error is 0.066m. At the beginning of the experiment, the depth of the experiment was measured as 15.2 m using an active sonar which shows good agreement with the passive estimation of the depth. However, slight variations might be observed due to the uneven rocky seabed and drifting of the hydrophones with ocean current.

In the experimental analysis described, power equalisation combined with MVDR beamforming significantly improves estimations of the depth of the seabed, as shown in Figure 8. From this figure, we can say that, using power equalisation and MVDR beamforming, a 4-hydrophone array provides a good estimate of the depth of the seabed using the frequency band of 200 to 1500 Hz. Although the large-bandwidth OAN is recorded to improve the SNR and resolution of the estimation in the passive fathometer, the noise fields at higher frequencies do not contribute to the passive fathometer due to the dominance of shrimp noises in shallow Australian waters.

However, the lower frequency band of 200 to 1500 Hz still shows consistency with theory shown in [28]. The SNR and resolution with respect to the bandwidth of the noise field are shown in Figure 9. The SNR is calculated as the ratio of the power of the correlation peak generated at about 13.5 ms to the variance in the correlation noise generated between 25 ms and 50 ms from the cross-correlation in Figure 8, and the resolution is calculated as the width (zero-crossing) of the correlation peak generated at about 13.5 ms in the cross-correlation.

Figure 9 shows that the relationship among the SNR, resolution and bandwidth is broadly consistent theories. Figure 9(a) shows that up to 1500Hz bandwidth SNR increases with an increase in bandwidth and it goes down for further increase of bandwidth due to shrimp as sound produced by them starts dominating in higher bandwidth. It also shows that both SNR and resolution using MVDR beamforming give better results compared to DS beamforming in the presence of shrimps, in particular, at higher frequencies. The SNR and resolution shown here is the average of five sets of data recorded from the same location.

4. CONCLUSIONS

The theoretical analysis of the passive fathometer in the presence of off-axis wind generated surface noise and shrimp noise, which affects estimations of the depth of the ocean, is explained in this paper. It is experimentally shown that the passive fathometer works well at a depth of about 15 m and on rocky bottom areas using equalised noise fields and MVDR beamforming in a 4-hydrophone array with a reasonable averaging time of 50 seconds. It is also shown that adaptive MVDR beamforming gives better estimations than conventional DS beamforming when keeping all other parameters the same. The SNR and resolution are both shown to improve with increased bandwidths of the hydrophones in the array, until sharp biological noise starts dominating in the OAN recorded at Jervis Bay, NSW, Australia. Analysis of the experimental data leads to an important conclusion about the usable bandwidth of the passive fathometer, that is, it is limited in Australian waters by broadband shrimp noise but not by the bandwidths of the hydrophones in the array.

5. REFERENCES

[1] C. H. Harrison. Sub-bottom profiling using ocean ambient noise. *J. Acoust. Soc. Am.*, 115(4):1505–1515, 2004.

[2] C.H. Harrison and D.G. Simons. Geoacoustic inversion of ambient noise: a simple method. *J. Acoust. Soc. Am.*, 112(4):1377–1389, 2002.

[3] J. E. Ehrenberg and T. C. Torkelson. Fm slide (chirp) signals: a technique for significantly improving the signal-to-noise performance in hydroacoustic assessment systems. *Fisheries Research, Elsevier*, 47:193–199, 2000.

[4] S. R. Pillai and H. S. Oh. A new estimation technique for near-shore bathematric measurements. *Signal Processing, Elsevier*, 80:809–818, 2000.

[5] T. Collins and P. Atkins. Nonlinear frequency modulation chirps for active sonar. *IEE Proc.-Radar Sonar Navig.*, 146(6):312–316, 1999.

[6] M. Siderius, C.H. Harrison, and M.B. Porter. A passive fathometer technique for imaging seabed layering using ambient noise. *J. Acoust. Soc. Am.*, 120(3):1315–1323, 2006.

[7] C. H. Harrison and M. Siderius. Bottom profiling by correlating beam-steered noise sequences. *J. Acoust. Soc. Am.*, 123(3):1282–1296, 2008.

[8] J. Traer, P. Gerstoft, and W. S. Hodgkiss. Ocean bottom profiling with ambient noise: A model for the passive fathometer. *J. Acoust. Soc. Am.*, 129(4):18251836, 2011.

[9] S.A. Albahrani, M.R. Frater, and E.H. Huntington. Linearly filtered estimation of the time-domain greens function from measurements of ambient noise (l). *J. Acoust. Soc. Am.*, 124(5):2699–2701, 2008.

[10] K. G. Sabra, P. Roux, and W. A. Kuperman. Emergence rate of the time-domain greens function from the ambient noise cross-correlation function. *J. Acoust. Soc. Am.*, 118:3524–3531, 2005.

[11] S.E. Fried, W. A. Kuperman, K. G. Sabra, and P. Roux. Extracting the local greens function on a horizontal array from ambient ocean noise. *J. Acoust. Soc. Am.*, 124(4):183–188, 2008.

[12] K. G. Sabra, P. Roux, A. M. Thode, G. L. DSpain, W. S. Hodgkiss, and W. A. Kuperman. Using ocean ambient noise for array self localization and self-synchronization. *IEEE J. Ocean. Eng.*, 30(2):338–347, 2005.

[13] P. Roux, W. A. Kuperman, and the NPAL Group. Extracting coherent wave fronts from acoustic ambient noise in the ocean. *J. Acoust. Soc. Am.*, 116:1995–2003, 2004.

[14] R. Snieder. Extracting the greens function from the correlation of coda waves: A derivation based on stationary phase. *Physical Review*, 69, 2004.

[15] R. L. Weaver and O. I. Lobkis. Fluctuations in diffuse fieldfield correlations and the emergence of the greens function in open systems. *J. Acoust. Soc. Am.*, 117(6):3432–3439, 2005.

[16] O. I. Lobkis and R. L. Weaver. On the emergence of the greens function in the correlations of a diffuse field. *J. Acoust. Soc. Am.*, 110(6):3011–3017, 2001.

[17] R. L. Weaver and O. I. Lobkis. Elastic wave thermal fluctuations, ultrasonic waveforms by correlation of thermal phonons. *J. Acoust. Soc. Am.*, 113(5):2611–2621, 2003.

[18] J. Ricket and J. Claerbout. Acoustic daylight imaging via spectral factorization: Helioseismology and reservoir monitoring. *The leading Edge*, 18(8):957–960, 1999.

[19] N. M. Shapiro and M. Campillo. Emergence of broadband rayleigh waves from correlations of ambient seismic noise. *Geophy. Res. Lett.*, Vol. 31:L07614, 2004.

[20] P. Gerstoft, W. S. Hodgkiss, M. Siderius, and C. H. Huang, C.F.and Harrison. Passive fathometer processing. *J. Acoust. Soc. Am.*, 123(3):1297–1305, 2008.

[21] Md. J. Alam, E. H. Huntington, and M. R. Frater. Effect of biological activity on broadband passive fathometry. *Open Journal of Acoustics*, 3(2A):39–49, 2013.

[22] M. Siderius, H. Song, P. Gerstoft, W. S. Hodgkiss, P. Hursky, and C.H. Harrison. Adaptive passive fathometer processing. *J. Acoust. Soc. Am.*, 127(4):21932200, 2010.

[23] Md. J. Alam, M.R. Frater, and E.H. Huntington. Improving resolution and snr of correlation function with the increase in bandwidth of recorded noise fields during estimation of bottom profile of ocean. Sydney, Australia, 24-27 May 2010.

[24] S.N. Sen. *Acoustics, waves and oscillations*. New age international, New Delhi, 1999.

[25] F. B. Jensen, W. A. Kuperman, M. B. Porter, and H. Schmidt. *Computational Ocean Acoustics*. American Institute of Physics, New Work, 1994.

[26] L. Jianheng and G. Tianfu. Model of wind-generated ambient noise in stratified shallow water. *Chinese Journal of Oceanology and Limnology*, 23(2):144–151, 2005.

[27] P. E. Holloway, G. Symonds, and R. N. Vaz. *Temperature and Salinity measurements in the Jervis Bay Region*. Department of Geography and Oceanography, Univeristy College, The University of New South Wales, Australian Defence Force Academy, 1992.

[28] Md. J. Alam, E. H. Huntington, and M. R. Frater. Tradeoff between bandwidth and number of array elements in the performance enhancement of passive fathometer. *Open Journal of Acoustics*, 3(2A):16–24, 2013.